Gardner-like crossover from variable to persistent force contacts in granular crystals

Lars Kool, Patrick Charbonneau, and Karen E. Daniels

Phys. Rev. E **106**, 054901 — Published 15 November 2022

DOI: 10.1103/PhysRevE.106.054901

Gardner-like crossover from variable to persistent force contacts in granular crystals

Lars Kool,[1,2] Patrick Charbonneau,[3] and Karen E. Daniels[2]

[1] *Laboratoire de Physique et Méchanique des Milieux Hétèrogènes, ESPCI, Paris, France*
[2] *Department of Physics, North Carolina State University, Raleigh, North Carolina 27695, USA*
[3] *Departments of Chemistry & Physics, Duke University, Durham, North Carolina 27708, USA*

(Dated: September 28, 2022)

We report experimental evidence of a Gardner-like crossover from variable to persistent force contacts in a two-dimensional, bidisperse granular crystal by analyzing the variability of both particle positions and force networks formed under uniaxial compression. Starting from densities just above the freezing transition, and for variable amounts of additional compression, we compare configurations to both their own initial state, and to an ensemble of equivalent, reinitialized states. This protocol shows that force contacts are largely undetermined when the density is below a Gardner-like crossover, after which they gradually transition to being persistent, being fully so only above the jamming point. We associate the disorder that underlies this effect to the size of the microscopic asperities of the photoelastic disks used, by analogy to other mechanisms that have been previously predicted theoretically.

INTRODUCTION

Granular materials differ from elastic solids in their response to external forces: rather than homogeneously supporting an applied load, the forces are transmitted by a sparse percolating network of particles [1–5]. If interparticle contacts are allowed to break, and the granular material yields, the topology of the force network changes even if no particle-scale rearrangement takes place [6, 7]. By contrast, if contacts are preserved, cyclic (un)loading does not affect the structure of the force network. While recent theoretical and numerical studies suggest the preservation of contacts might not coincide with the jamming transition [8, 9], it is yet to be experimentally verified whether such a distinction exists.

The distinction between the onset of contact memory and jamming is reminiscent of the critical transition reported for certain amorphous solids and crystals of slightly polydisperse particles [10–16]. The associated Gardner transition is often depicted using an energy landscape roughened by a hierarchy of metastable basins. Outside of the Gardner regime, the energy scales are well-separated from the landscape roughness, and the system responds elastically [17]. By contrast, within the Gardner regime, the landscape roughness gives rise to easier pathways to escape from marginally stable sub-basins and thus to minute structural rearrangements (much smaller than the particle scale) that result in a different spatial distribution of contact forces at jamming [12, 18].

This landscape roughness in the Gardner phase also leaves a dynamical signature. Outside of the Gardner regime, the long-time mean squared displacement (MSD) Δ of the constituent particles plateaus at a value that depends on the particle cage size (and thus density/pressure for a hard sphere system) [8]. By contrast, within the Gardner regime, particles can't effectively sample the landscape over accessible time scales, which results in a MSD that doesn't saturate with time. Its asymptotically long-time value can nevertheless be estimated from the distance Δ_{AB} between two system copies, A and B, that started from the same reference configuration at a density below the Gardner regime and then evolved along different stochastic trajectories. One can thus define the Gardner regime as the density for which $\Delta < \Delta_{AB}$ at (sufficiently) long times. This was first shown experimentally in a granular glass former by Seguin and Dauchot [19], who captured a signature of Gardner physics in the dynamics of a vibrated, two-dimensional (2D), disordered packing of granular disks. More recently Xiao et al. [20] found signatures of Gardner physics in quasi-thermal (air-fluidized) star-shaped particles. However, the corresponding contact force network has not been observed experimentally, nor have the factors that control the distance of the Gardner transition to jamming been assessed [12].

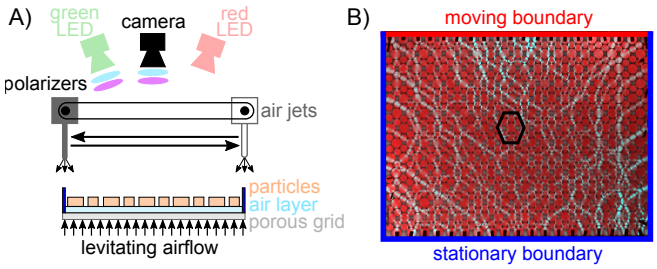

FIG. 1. A) Schematic of the experimental setup, side view, with the height of the air layer not to scale. B) Typical image (top view) from which the particle positions (red channel) and force transmission (cyan channel) are extracted. The hexagon marks an H1 unit cell [21].

In this article, we investigate the crossover from variable to persistent contacts in a granular crystal (see Fig. 1). We find that this transition is strongly analogous to that predicted by Gardner physics, is clearly distinct from the jamming transition, and that the distance between the two appear here to be controlled by the scale of the microscopic asperities of the experimental disks.

METHODS

Despite numerical studies of ultrastable glasses [22] and polydisperse crystals [12] which successfully suppress particle-scale rearrangements to reveal the Gardner regime, it remains an open challenge to translate these numerical protocols for generating ultrastable glasses to experiments. We, instead, study marginally-stable states generated from a well-defined 2D crystalline packing to suppress rearrangements via an alternative means. We selected the H_1 crystal symmetry, containing a unit cell of three large and six small disks (see Fig. 1), from among those identified by [21], for having no basis vectors aligned with the compression axis. This choice thereby limits the putative contribution of low-energy, local buckling excitations [15, 23–25], and focuses the dynamics on the quenched disorder that arises through variability in particle size and surface roughness [12]. We found that this crystal successfully suppresses rearrangements; when one does occur, the system can readily be reinitialized. Although the resulting crystalline axes create an additional coordinate system that is neither orthogonal nor aligned with the natural axes of the apparatus (see Fig. 1), we are able to account for these effects during the data analysis.

We performed our experiments on a single-layer packing of bidisperse photoelastic disks ($N_S = 507$ small disks with $R_S = 5.5$ mm and $N_L = 273$ large disks with $R_L = 7.7$ mm, Vishay PhotoStress PSM-4) with a reflective back layer levitated on a gentle layer of air forced through a porous grid; this setup has been previously described in [26, 27]. By reducing basal friction, such that interparticle forces dominate, particles are free to explore their cages and sample available configurations under gentle perturbations. We randomize particle positions *within their cage* by sweeping a turbulent airflow across the upper surface of the packing (see Fig. 1a); time is measured in units of these $t_r = 20$ s randomization sweeps. We explore cage sizes and separations as a function of density ϕ by uniaxially compressing the system in discrete increments of $\delta\phi/\phi = 6 \times 10^{-4}$, moving one boundary with a stepper motor. Each of the four boundaries are laser-cut from acrylic sheets. The particles along both the moving boundary, and the static boundary opposite, are pinned to suppress large-scale crystal rearrangements.

Particle positions and the network of interparticle forces were imaged using a single camera and two light sources: an unpolarized red LED light for the positions, and a circularly-polarized green LED light for the photoelastic visualization of stresses (see Fig. 1b). We located the centroid of each particle using the convolution of the red channel of the image with a predefined mask matching the particle size [28, 29]; this allows us to determine locations within ≈ 0.1 px ($\approx 1/250\ R_L$) precision. Because we are studying well-defined crystal configurations, for which all particle displacements are at least an order of magnitude smaller than the particle size, we were able to bypass traditional particle-tracking algorithms and their caveats. Each particle position was instead determined from the first image, hand-checked for completeness, and then used as a reference position for subsequent images. Within these images, the sole particle located within R_L of the reference particles was attached to its trajectory. To minimize edge effects, particles within $4R_L$ of the walls were discarded from the dataset, leaving $N_p = 628$ particles for our analysis.

RESULTS

Gardner crossover

We have adapted the protocol of [19] to identify transitions in the cage dynamics as a function of ϕ, using overhead airjets to randomly promote cage exploration rather than supplying a global vibration of the bottom plate. We determine the cage dynamics at 20 different ϕ, equally spaced between $\phi_{\min} = 0.8006 \pm 0.0002$ (the limit of mechanical stability of the crystal) and $\phi_{\max} = 0.8162 \pm 0.0002$ (slightly larger than ϕ_J, guaranteeing that the Gardner regime is traversed but without activating the out-of-plane buckling mode that develops deeper into the jammed phase). From an initial state at $\phi_{\min}$, the system is compressed to $\phi_{\max}$, and then decompressed step-wise and allowed to equilibrate for $t = 100t_r$ at each intermediate density. Upon reaching $\phi_{\min}$, the system is deemed *reinitialized*. We performed a total of 10 initializations, shown schematically in Fig. 2A.

For each ϕ, the cage separation distance Δ_{AB} is obtained by comparing particle positions between two different initializations, A and B, taken at the same ϕ:

$$\Delta_{AB}(t;\phi) = \frac{1}{N_p}\sum_{i=1}^{N_p} |\mathbf{r}_i^B(t) - \mathbf{r}_i^A(t)|^2 \qquad (1)$$

where $\mathbf{r}_i^\alpha(t)$ is the position of particle i at time t in initialization α. The cage size Δ (within a single initialization A) at a given ϕ is obtained from particle displacements after a long experimental time of $100t_r$, according to

$$\Delta(t;\phi) = \frac{D}{N_p}\sum_{i=1}^{N_p} |\mathbf{r'}_{i,y}^A(t) - \mathbf{r'}_{i,y}^A(0)|^2. \qquad (2)$$

In both cases, the average at each ϕ over all runs is then calculated, denoted by $\langle\cdot\rangle$. The corrections D and $\mathbf{r'}$ in Eq. (2) ensure that $\langle\Delta\rangle = \langle\Delta_{AB}\rangle$ in the vicinity of $\phi_{\min}$; they are experimentally motivated as follows. First, even at $\phi_{\min}$ the MSD of a caged particle plateaus at longer times than are experimentally accessible; we measured this time to be $\approx 1000t_r$, while our experiments can only reach $100t_r$. Because we expect the relative ratio of these lengthscales to be constant at low ϕ, we have rescaled our measurement of Δ by the ratio $D = 1.2$, our estimate of this ratio [30]. Second, we observed that for $\phi > \phi_G$,

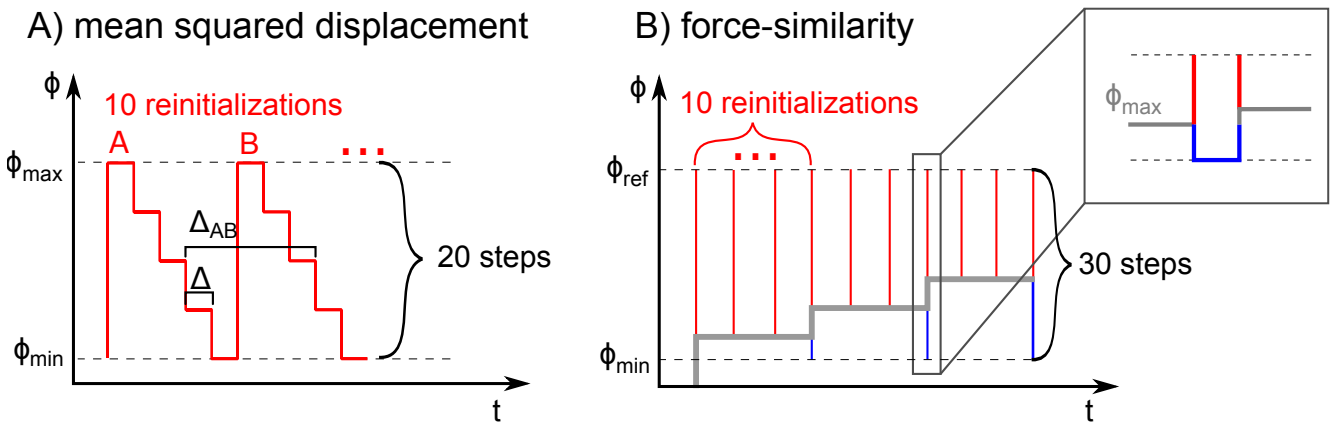

FIG. 2. A) Schematic representation of the protocol used to determine the cage size, Δ, and the mean cage separation, Δ_{AB}, via the MSD. B) Schematic representation of the protocol used to determine the persistence of inter-particle contacts, via the force-similarity analysis.

histograms of the (x, y) displacements displayed multiple distinct peaks, each aligned with the direction of one of the lattice vectors of the unit cell, rather than being azimuthally symmetric around zero, as observed for $\phi < \phi_G$. To correct for the biased motions introduced by the crystalline axes that give rise to these peaks, we applied a linear transformation to orthogonalize the system. Equation (2) therefore defines Δ as the MSD of the Gaussian part of the displacement (along the y'-axis) in the orthogonalized system r'_y, and ignores the displacements along the more-complicated (x') axis [30].

Figure 3 presents the histograms of Δ and Δ_{AB} measured at various ϕ. At low ϕ, the statistical distributions of Δ and Δ_{AB} are nearly identical, which is characteristic of a normal solid. In contrast, for $\phi \gtrsim 0.807$ we observe that $\langle\Delta\rangle < \langle\Delta_{AB}\rangle$, indicating the onset of a Gardner-like regime at $\phi_G = 0.807 \pm 0.0005$. As ϕ further increases, force chains emerge, thus identifying the jamming point, $\phi_J = 0.8100 \pm 0.0005$ (Fig. 4C); this value is determined by measuring the average proportional change of the pixel intensity I_g of the photoelastic (green) channel above the minimum observed value [30]. Note that, although we expect $\Delta = 0$ in the jammed phase, a finite value is measured; this captures the noise floor of our system and analysis.

Inter-particle forces

Having identified a Gardner-like crossover using the particle displacement data, we now separately consider the evolution of inter-particle forces within each (marginally stable) state at different ϕ. We observe changes in the persistence of the photoelastic fringes (as proxy for inter-particle forces, see Fig. 4A-B), of a given state by compressing the system to a jammed reference density $\phi_{\rm ref} = 0.8147 \pm 0.0002$, which is slightly above $\phi_{\rm max} = 0.8127 \pm 0.0002$, at which a better imaging is obtained. All values of ϕ were measured during *a posteriori* image analysis, and thus do not necessarily match between the two types of experiments. The lowest densities for MSD measurements, $\phi_{\rm min} = 0.8006$ and for force-similarity measurements, $\phi_{\rm min} = 0.8002$, are nevertheless identical within measurement error, but the densest system for MSD measurements, $\phi_{\rm max} = 0.8162$, was significantly denser than for force-similarity measurements, $\phi_{\rm max} = 0.8127$. This difference arises from the observation that deep in the jammed phase, forces become more homogeneous, thus making it harder to detect changes. Choosing $\phi_{\rm max}$ for force-similarity measurements closer to ϕ_J therefore makes changes in the fringes more apparent. In both experiments, $\phi_{\rm max}$ is nevertheless above the determined jamming density $\phi_{\rm J} = 0.8100$. In this context, because the system is arrested above ϕ_J and the contact network is fully formed, the difference in $\phi_{\rm max}$ is not deemed significant. For systems with few interparticle contacts, the correlation between fringes is dominated by noise, whereas in well-jammed systems the force network is completely percolated (due to the crystalline nature of the system), thus making changes to the force network insignificant compared to the average inter-particle force.

Changes in the photo-elastic fringes at $\phi_{\rm ref}$ are determined as follows. We first image the photoelastic fringes of the initial state, $\mathcal{I}$. The system is then decompressed to $\phi_{\rm min} < \phi < \phi_{\rm max}$, and evolved for $10t_r$ (sufficient for the force network to randomize), before recompressing to $\phi_{\rm ref}$ and to image the photoelastic fringes of this final state, $\mathcal{F}$. We repeat this protocol for 30 equidistant densities within the interval $[\phi_{\rm min}, \phi_{\rm max}]$. In all cases, the system is decompressed to $\phi_{\rm min}$ before moving to the next ϕ to erase any memory of the previous experiment. The protocol is schematically represented in Fig. 2B. We quantify the degree of similarity between the $\mathcal{I}$ and $\mathcal{F}$ states for a given ϕ using a normalized cross-correlation

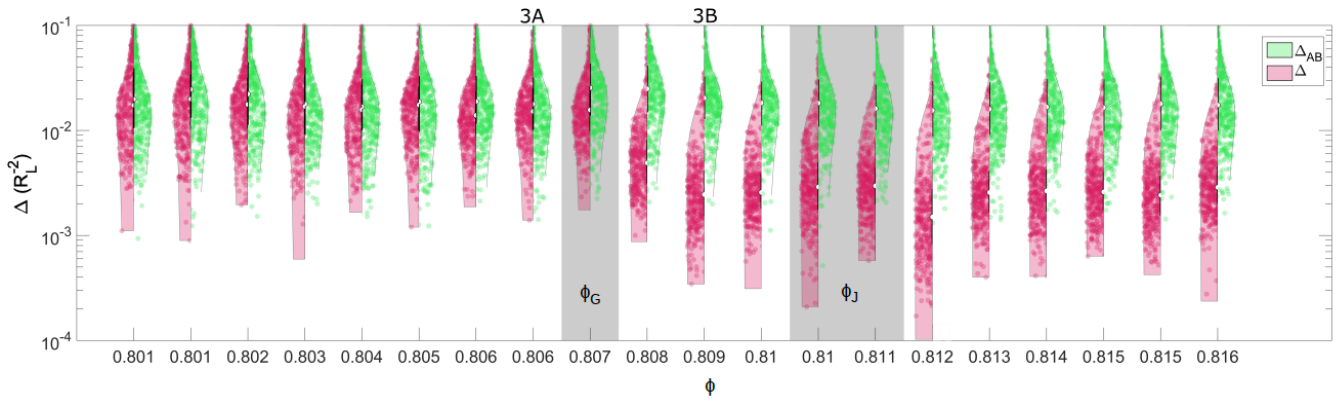

FIG. 3. Side-by-side histograms of the probability density functions of Δ (magenta, left) and Δ_{AB} (green, right) measured at each density ϕ. Both Δ and Δ_{AB} are non-dimensionalized using the radius of the large particle, R_L. At $\phi < \phi_G$ (crossover denoted by gray rectangle), the histograms of Δ and Δ_{AB} agree (both in mean and width of the distribution), whereas for $\phi > \phi_G$, we see that $\Delta < \Delta_{AB}$. Above the jamming point ϕ_J (transition denoted by gray rectangle), the histograms of Δ and Δ_{AB} differ markedly. Histograms 3A and 3B correspond to the two snapshots presented in Fig. 4.

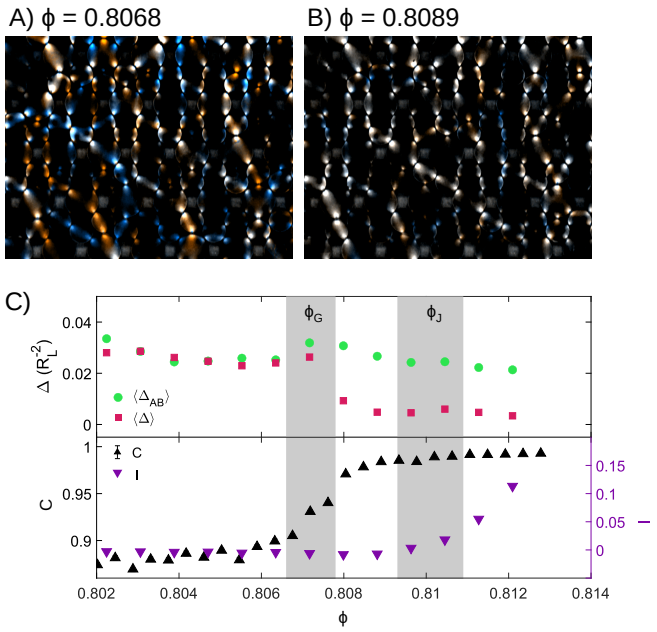

FIG. 4. Overlay of two marginally stable states (red and blue) and their overlap (white) for (A) $\phi < \phi_G$ and (B) $\phi > \phi_G$. The two states have little overlap for $\phi < \phi_G$, whereas for $\phi > \phi_G$ the two states have a large overlap between their force network. A movie of overlays with increasing density makes this point even more saliently [30]. (C) Overlay of $\langle\Delta\rangle$ (magenta ■) and $\langle\Delta_{AB}\rangle$ (green •) as a function of ϕ on the top axis; force correlation C (black ▲) and fringe intensity I (purple ▼) on the bottom axis, both as function of ϕ. Both Δ and Δ_{AB} are non-dimensionalized using the radius of the large particle, R_L.

of the photoelastic fringes, taken $10t_r$ apart:

$$C(\phi) = \left\langle \frac{\sum_{x,y}[\mathcal{I}_i(x,y) - \overline{\mathcal{I}}_i][\mathcal{F}_i(x,y) - \overline{\mathcal{F}}_i]}{\sqrt{\sum_{x,y}[\mathcal{I}_i(x,y) - \overline{\mathcal{I}}_i]^2 \sum_{x,y}[\mathcal{F}_i(x,y) - \overline{\mathcal{F}}_i]^2}} \right\rangle \tag{3}$$

with $\mathcal{I}_i(x,y)$ the pixel intensity of pixel (x,y) of particle i, $\overline{\mathcal{I}}_i$ the average pixel intensity of particle i in state $\mathcal{I}$, and the average, $\langle\cdot\rangle$, running over all particles in all pairs $\mathcal{I}$ and $\mathcal{F}$ of states at a given ϕ.

Figure 4 shows two superimposed images of force chains: $\mathcal{I}$ (blue) obtained before the airjet sweeps, and $\mathcal{F}$ (red) after, such that white denotes regions where force chains did not change, while red and blue denote force chains present in only one of the two images. For $\phi < \phi_G$ (Fig. 4A) the rare force chain overlaps (white) indicate that inter-particle contacts remain variable at low ϕ. In contrast, for $\phi > \phi_G$ (Fig. 4B) white regions dominate, indicating that inter-particle contacts persist. Similar images obtained over the full density range further reveal that force-chain rearrangements are long-range, even though the particle rearrangements are not [30].

Figure 4C compares these perspectives, showing $\langle\Delta\rangle$ and $\langle\Delta_{AB}\rangle$, the measure for inter-particle forces $\langle I_g\rangle$, and the normalized cross-correlation C, all as a function of ϕ. Note that we chose the average green channel intensity $\langle I_g\rangle$ as a measure for the inter-particle forces because standard force detection algorithms do not work well on the minute contact forces present at the onset of jamming. This choice is further motivated by noting that $\langle I_g\rangle$ scales linearly with the applied load at low loads [30, 31]. This plot therefore shows that the onset of the Gardner-like regime (for which $\langle\Delta\rangle < \langle\Delta_{AB}\rangle$) coincides with the onset of the conservation of inter-particle contacts (given by the sharp rise in C), and is distinct from ϕ_J (defined in the onset of the rise of $\langle I_g\rangle$, suggesting that the force network gets increasingly determined as soon as $\phi > \phi_G$.

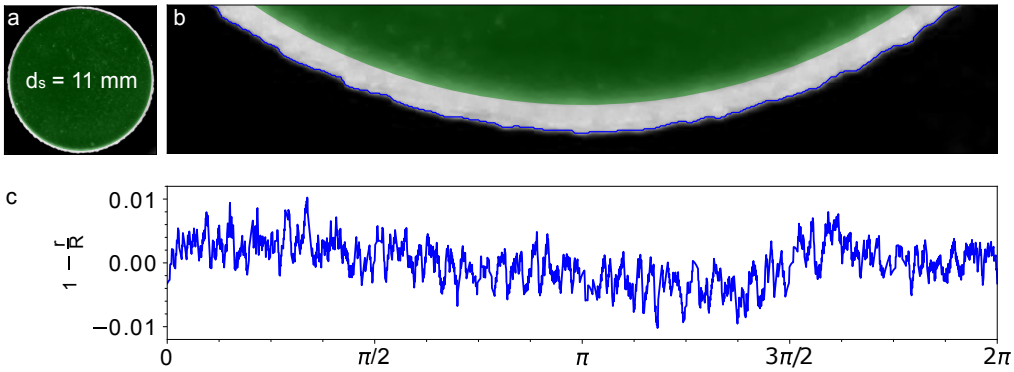

FIG. 5. (a) Micrograph of a single photoelastic particle that is (b) enlarged so as to illustrate the edge-detection (blue); the green circle traces a perfect circle for reference. (c) Fractional deviation of the particle edge r from the average radius R along the circumference.

By analogy to what has been reported for numerical simulations of size-polydisperse particles in otherwise crystalline systems [12], we expect the distance to jamming to be controlled by particle disorder. Given that all particles were cut from flat sheets with the same fixed-radius metal cutter [29], disorder is here expected to be dominated by irregularities along the disk edges (see Fig. 5). Generalizing the polydispersity argument of [12] to this case, we expect the onset of the Gardner regime to be set by the particles' dimensionless deviation from a constant radius:

$$\sqrt{\phi_J - \phi_G} \propto 1 - \frac{r}{R}. \tag{4}$$

Two key features emerge from the image analysis: asphericity of $\sim 1\%$, superimposed with a surface roughness of $\sim 0.3\%$. Both quantities are of the same order of magnitude as the relative distance between the Gardner-like crossover in and the jamming point for our system, $s = \sqrt{0.810 - 0.807} \approx 1\%$. Because our particles were all cut using the same fixed-radius metal cutter, they have similar irregularities along the disk edges. A systematic investigation of particle roughness is therefore not possible for this system and is left for future consideration.

CONCLUSION

We have shown that small particle irregularities—always present in experiments but often neglected—in an otherwise crystalline system exhibit Gardner-physics-like features near jamming. Although 2D systems are expected not to exhibit proper Gardner criticality [13], the finite size of our system suppresses the long wavelength fluctuations that would normally occlude this effect in the thermodynamic limit, thus preserving some of its physical features. This choice of system further allowed us to study changes in the force network of one specific configuration, where we found experimental evidence correlating the onset of that regime to the determination of force contacts near jamming. For the particles we used, the distance from jamming of the Gardner crossover was similar to the inherent roughness of the particles, a finding consistent with the study of size polydispersity in Charbonneau et al. [12].

Future work should measure the role of irregularities directly, perhaps through the printing of particles with systematically-controlled roughness. This work motivates delving further into the influence of particle roughness on a micromechanical level. Whereas surface roughness has been investigated on a macroscopic level, such as for relating surface roughness and friction in glass spheres [32, *e.g.*], we showed that roughness could also influence interactions on a microscopic level. This finding raises questions about what signatures of frictional jamming found for smooth particles [33] match those needed to describe, more realistic, rough particles [34]. In this context, including geometrical asperities [35] in numerical simulations could provide particularly invaluable insight.

ACKNOWLEDGMENTS

We thank Sho Yaida, Jonathan Kollmer, and Eric Corwin for motivating discussions, Joshua Dijksman for help with image processing, and Jonathan Kollmer, Clayton Kirberger, and Josh Miller for technical assistance. PC acknowledges support from the Simons Foundation, Grant No. 454937. KD acknowledges support from NSF DMR-0644743 (apparatus) and current support from DMR-2104986. LK acknowledges support from the European Union's Horizon 2020 research and innovation programme *Caliper*, Marie Skłodowska Curie Grant No. 812638.

[1] P. Dantu, Géotechnique **18**, 50 (1968).

[2] H. M. Jaeger, S. R. Nagel, and R. P. Behringer, Reviews

of Modern Physics **68**, 1259 (1996).
[3] F. Radjai, D. E. Wolf, M. Jean, and J.-J. Moreau, Physical Review Letters **80**, 61 (1998).
[4] D. Howell, R. P. Behringer, and C. Veje, Physical Review Letters **82**, 5241 (1999).
[5] J. Peters, M. Muthuswamy, J. Wibowo, and A. Tordesillas, Physical Review E **72**, 041307 (2005).
[6] B. P. Tighe, J. H. Snoeijer, T. J. Vlugt, and M. van Hecke, Soft Matter **6**, 2908 (2010).
[7] J. E. Kollmer and K. E. Daniels, Soft Matter **15**, 1793 (2019).
[8] P. Charbonneau, J. Kurchan, G. Parisi, P. Urbani, and F. Zamponi, Annual Review of Condensed Matter Physics **8**, 265 (2017).
[9] P. Charbonneau and P. K. Morse, Physical Review Letters **126**, 088001 (2021).
[10] E. Gardner, Nuclear Physics B **257**, 747 (1985).
[11] J. Kurchan, G. Parisi, P. Urbani, and F. Zamponi, The Journal of Physical Chemistry B **117**, 12979 (2013).
[12] P. Charbonneau, E. I. Corwin, L. Fu, G. Tsekenis, and M. van Der Naald, Physical Review E **99**, 020901 (2019).
[13] L. Berthier, G. Biroli, P. Charbonneau, E. I. Corwin, S. Franz, and F. Zamponi, The Journal of Chemical Physics **151**, 010901 (2019).
[14] P. Charbonneau, J. Kurchan, G. Parisi, P. Urbani, and F. Zamponi, Nature Communications **5**, 3725 (2014).
[15] G. Tsekenis, EPL (Europhysics Letters) **135**, 36001 (2021).
[16] A. P. Hammond and E. I. Corwin, Proceedings of the National Academy of Sciences **117**, 5714 (2020).
[17] G. Biroli and P. Urbani, Nature Physics **12**, 1130 (2016).
[18] Y. Jin and H. Yoshino, Nature Communications **8**, 1 (2017).
[19] A. Seguin and O. Dauchot, Physical Review Letters **117**, 228001 (2016).
[20] H. Xiao, A. J. Liu, and D. J. Durian, Physical Review Letters **128**, 248001 (2022).
[21] C. Likos and C. Henley, Philosophical Magazine B **68**, 85 (1993).
[22] L. Berthier, P. Charbonneau, Y. Jin, G. Parisi, B. Seoane, and F. Zamponi, Proceedings of the National Academy of Sciences **113**, 8397 (2016).
[23] E. Lerner, G. Düring, and M. Wyart, Soft Matter **9**, 8252 (2013).
[24] P. Charbonneau, Y. Jin, G. Parisi, C. Rainone, B. Seoane, and F. Zamponi, Physical Review E **92**, 012316 (2015).
[25] P. Charbonneau, E. I. Corwin, G. Parisi, and F. Zamponi, Physical Review Letters **114**, 125504 (2015).
[26] J. G. Puckett and K. E. Daniels, Physical Review Letters **110**, 058001 (2013).
[27] E. S. Bililign, J. E. Kollmer, and K. E. Daniels, Physical Review Letters **122**, 038001 (2019).
[28] J. Kollmer, *Photo-elastic grain solver*, URL `https://github.com/jekollmer/PEGS`.
[29] K. E. Daniels, J. E. Kollmer, and J. G. Puckett, Review of Scientific Instruments **88**, 051808 (2017).
[30] See Supplementary Material for a schematic overview of the protocols, details about the MSD correction and orthogonalization schemes, the jamming point determination, and a movie of force contact overlaps.
[31] A. Abed Zadeh, et al., Granular Matter **21**, 4, 1–12 (2019).
[32] S. Utermann, P. Aurin, M. Benderoth, C. Fischer, and M. Schröter, Physical Review E **84**, 031306 (2011).
[33] L. E. Silbert, D. Ertaş, G. S. Grest, T. C. Halsey, and D. Levine, Physical Review E **65**, 031304 (2002).
[34] S. Pradeep, M. Nabizadeh, A. R. Jacob, S. Jamali, and L. C. Hsiao, Physical Review Letters **127**, 158002 (2021).
[35] S. Papanikolaou, C. S. OHern, and M. D. Shattuck, Physical Review Letters **110**, 198002 (2013).